

# A NUMERICAL SOLAR MODEL

C. M. BARRETT<sup>\*</sup>, A. N. HOCK<sup>\*</sup>, J. M. SANDERS<sup>∇</sup>

## Abstract

A basic model of stellar structure is presented here. The sun is initially modeled using four fundamental equations of stellar structure. Since these equations are not analytically solvable, they were solved numerically using the Runge-Kutta fourth order approximation. Despite several first-order approximations that were made, resulting values for density, mass, luminosity, and temperature were correct to relative error on the order of  $10^{-7}$ . The inclusion of variable chemical composition increased the accuracy of the model further still. The internal error of the numerical analysis was also on the order of  $10^{-7}$ , which showed the dependability of our rudimentary models. Throughout, the mechanisms of opacity and energy generation in the stellar model are addressed.

## Introduction

The equations of stellar structure from Carroll's *Modern Astrophysics* are used here in conjunction with numerical analysis tools to describe a quantitative stellar model. The goal, by the end of the first round of calculations, was to have a basic but elucidating model of the Sun. The assumptions made in this stage were made in an effort to retain ease in analysis. The Sun was assumed to be spherical with equal compositions and dynamics radiating out from the center. Also, complete ionization of a constant composition atmosphere was assumed. Finally, solar convection was calculated to have negligible effects so it was neglected in favor of simplicity and ease of calculation. We then set out to construct a giant or super-giant star of spectral type O or B. In that type of hot, high mass star, we expected to see a good deal of convection, so the value of programming in convection could be readily analyzed.

In both models, non-linear differential equations were needed to approximate the radius-dependent density, mass, luminosity, and temperature. The four coupled equations are shown below, and the Runge-Kutta fourth order numerical approximation was used to solve for each aspect of the model star. In the worksheet incorporating convection, the representation of the temperature gradient was altered to reflect the changing nature of energy transport. The general equations are:

---

<sup>\*</sup> Colgate University Undergraduate Studies, Department of Physics and Astronomy

<sup>∇</sup> Colgate University Undergraduate Studies, Department of Chemistry

$$\frac{dp}{dr} = \left[ \frac{-G \cdot M \cdot \rho}{r^2} + \frac{3 \cdot \kappa(\rho, T) \cdot \rho \cdot L}{4 \cdot a \cdot c \cdot T^3 \cdot 4 \cdot \pi \cdot r^2} \cdot \left\{ \frac{k \cdot \rho}{\mu \cdot m_H} + \frac{4}{3} \cdot a \cdot T^3 \right\} \right] \cdot \frac{\mu \cdot m_H}{k \cdot T}$$

$$\frac{dM}{dr} = 4 \cdot \pi \cdot r^2 \cdot \rho$$

$$\frac{dL}{dr} = 4 \cdot \pi \cdot r^2 \cdot \rho \cdot \epsilon(\rho, T)$$

$$\frac{dT}{dr} = \frac{-3 \cdot \kappa(\rho, T) \cdot \rho \cdot L}{4 \cdot a \cdot c \cdot T^3 \cdot 4 \cdot \pi \cdot r^2}$$

The equation for the density gradient was derived from  $dP/dr$ , or the equation of hydrostatic equilibrium. The mass differential is a modified version of the conservation of mass and describes how mass interior to a given radius must increase with increasing distance from the origin. The luminosity generated internal to a given value of  $r$  is given by  $dL/dr$ . This equation is essentially the conservation of energy, where  $dL$  is the differential energy contribution of an infinitesimally thin spherical shell. The last of the four basic equations of stellar structure is that of the temperature gradient for radiative transport. In the initial model of the sun, the contributions of convection were neglected (this assumption is proved valid later), so the temperature gradient due to convective transport was not included in the derivative matrix used to model the sun. Note that with an increase in luminosity, density, or opacity, the temperature gradient must become more severe in order to transport all of the energy to the surface of a star. It is during these times of increased opacity and energy generation that convection becomes vital. The derivative must include a piece of code to incorporate the switch between radiative and convective transport; this is shown later in the model of the blue giant star, where conditions favor convection.

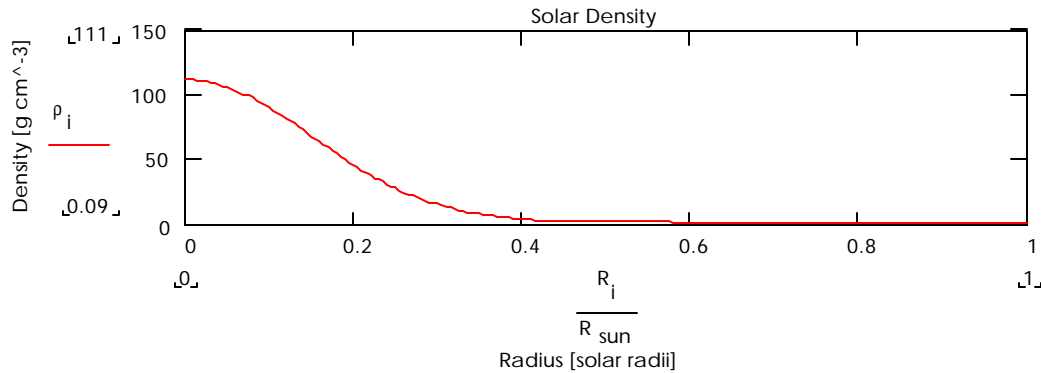
Note that each of the equations has at least one dependent variable that is contained in another one of the equations. In the same sense, the four differential equations are *coupled* and must be solved as a group. Though many more equations go into an elegant, research-level stellar model, one can construct an illuminating model with only these equations. The input of information about the physical properties of the star, and boundary conditions make this derivative matrix numerically solvable by Mathcad. The constitutive relations concerning opacity and energy generation were used with the approximation of constant composition and complete ionization throughout the star. The approximation of constant composition, as will be seen later in this study, was the worst assumption made. Varying composition has a direct effect on pressure, opacity, and energy generation. Boundary conditions were implemented through the "initial condition matrix" used by Mathcad. Inherent in the values used for this matrix are the assumptions that: 1) at the core,  $M=0$  and  $L=0$ , 2) at the edge of the star,  $T$ ,  $P$ , and density all fall off to zero in the interstellar medium. More sophisticated boundary conditions would result in a better model, but at this level these assumptions result in a very illuminating study.

A brief explanation of the Rkadapt function used by Mathcad is also necessary before delving in to the functional aspects of this project. This function, hardwired into the Mathcad software, allows the input of a derivative matrix, and the output of iterated solution values for the dependent variables. The user is responsible for the input of initial conditions for the dependent variables, and the input of boundary conditions for the independent variable. One of the unique features of Rkadapt is that has the ability to vary the spatial resolution of its numerical approximations if the function is one that changes abruptly over short time scales. For this project, the four differential equations are listed above, and the initial condition matrix is actually one of internal boundary conditions. For instance, at the edge of a star, we assume that density and temperature are at a minimum, but where  $R=0$ , density and temperature are at a maximum. So when modeling a hypothetical star, changing the boundary conditions until a reasonable model formed was necessary. As an example, one aspect of the Vogt-Russel Theorem shows that the initial condition of a star (including composition) has a great deal of influence on it over an entire lifetime.

# I. Solar Model

## A. Results from the Runge-Kutta Analysis:

All equations were laid out as mentioned above, and include given constants. In terms of hard results received from the numerical analysis, the most profitable analysis sometimes comes directly from graphic interpretation. In this spirit, graphs were made illustrating density, mass, luminosity, temperature, opacity, and energy generation.



The density change with respect to radius,  $\frac{d\rho}{dr}$ , is governed by a combination of terms derived from  $\frac{dP}{dr}$ . In modeling of different size stars, this curve sometimes exhibits a "hump" where  $\rho$  increases above the initial values. An effort was made to classify the shape of this curve and its physical significance. In part, this was done to try to understand where this density increase comes from in larger stars. From the description of radiation pressure:

$$\frac{d\rho}{dr} \propto -c_1(\rho, M, T^{-1}) \frac{dP}{dr} + c_2(\rho, T^3) \frac{dT}{dr}$$

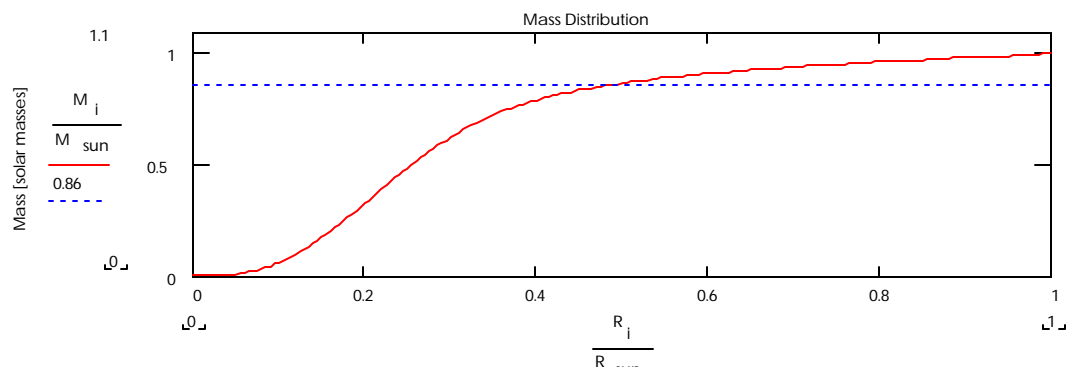
where terms for radiation pressure and gas pressure are included in  $p(r)$ . In general, we see that the density gradient is determined by the interaction of  $\frac{dP}{dr}$  and  $\frac{dT}{dr}$ . Getting rid of the cumbersome constants, and

$$\frac{dP}{dr} = \frac{kT}{\mu m_H} \frac{d\rho}{dr} + \frac{k\rho}{\mu m_H} \frac{dT}{dr} + \frac{4}{3} aT^3 \frac{dT}{dr}$$

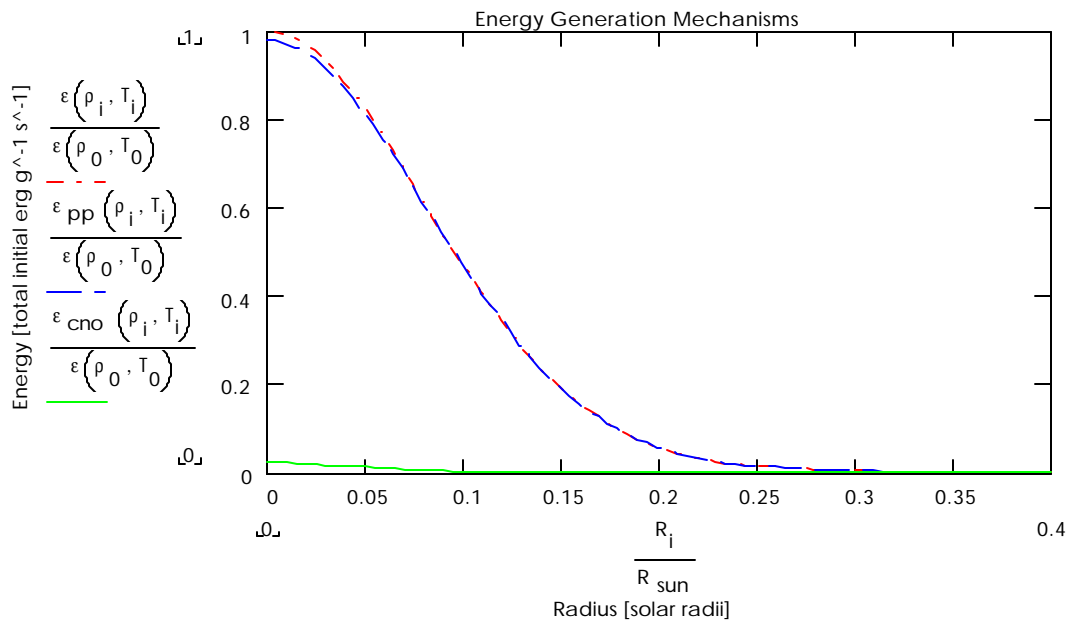
using proportionality, the above equation becomes:

where the constants  $c_1$  and  $c_2$  are dependent on the variables shown. So, after this brief analysis, one can see that  $\frac{d\rho}{dr}$  will be positive for regions of the stellar envelope where the temperature is high enough (i.e. just outside the core of a large star). In some stellar models, the density increase just outside the core is very pronounced; in many of these cases, convection and opacity (radiation pressure) play a significant role in supporting  $\rho$  as  $R$  increases. Due to our poor rendition of opacity, though, the density does not drop off as quickly as expected (see Carroll fig 11.7).

Below is the graph representing mass distribution in the Sun. It shows strong correspondence to the fact that nearly all of the Sun's mass is contained within the first half of the radius. Note on the plot where  $M(R_{sun}/2) \sim 85\%$  of the total mass; if our opacity model were more accurate, one would likely see



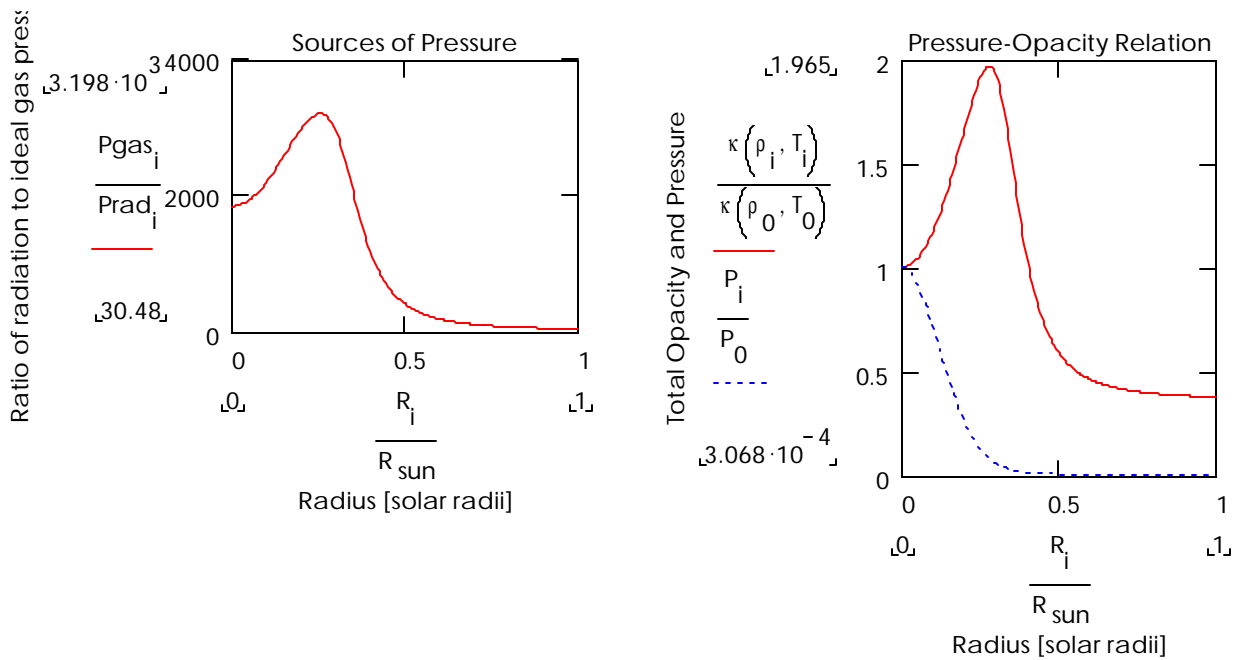




the top solid curve is the total opacity (via free-free, bound-free, and electron-scattering). One can see that the free-free opacity dominates over the other two mechanisms until about half way through the sun, where electron scattering provides most of the opacity. One can note from the plot of opacity mechanisms that: 1) bound-free interactions are rare throughout the radius of the sun. In fact, the peak opacity due to b-f is only about 10% of the total around 0.3 solar radii. This is due to our approximation of total ionization in the atmosphere and the lack of bound atoms. 2) Electron-scattering is independent of density and temperature. After about 0.5 solar radii, electron scattering is the primary mechanism driving opacity, and continues throughout the rest of the sun at a constant value of ~40% of the initial opacity. The relative increase in the contribution of e-s opacity here is due to the lower temperature and density, so kff is less effective. One of the overall weaknesses of this model is the approximation of opacity. By using varying composition, as is more accurate (see Carroll fig. 11.3), the results from above could be improved.

### C. Pressure Sources in the Sun:

In consideration of all the different mechanisms that effect the interior structure of the sun, it may be helpful to perform an analysis of the different types of pressure individually. The effects of degeneracy in the sun are assumed negligible; ideal gas pressure (thermal) and radiation pressure have been plotted below. However radiation pressure should be negligible according to our previous investigation of opacity in the sun. The pressure-opacity relation is an interesting one for several reasons. It shows, initially, that opacity is roughly proportional to the pressure. This is seen as opacity continues to rise until the internal pressure falls to around zero. The constant value for electron scattering (which would not be constant for changing stellar composition) provides most of the amplitude, whereas pressure (i.e. temperature and density) dictates the shape of the continuum opacity. As long as the assumption of constant composition remains in place, I expect to see this type of structure in any stellar model. In this solar model, the radiation pressure is effectively zero; the ideal gas pressure in the sun is more than 1000 times greater than the radiation pressure for almost 50% of the radius. To clarify the role radiation pressure plays in the sun, and to relate it more effectively to later models, a plot of radiation pressure over gas pressure is also shown. In the plot above, the minor role that radiation pressure plays is truly evident.



#### D. Accuracy Checks:

In order to check the accuracy of these graphs, several checks have been implemented to see gives an approximate value for the integrated original differential equations, and the resulting values can be compared to the Nth value given by Rkadapt. Therefore, the Simpson method provides a check of the numerical method used.

The rudimentary checks above say that our numerical values are correct to better than an order of magnitude. “Very often we need to be able to integrate a function for which we have no analytic form, but only evenly spaced samples. Simpson’s method is a nice compromise between ease of implementation and

$$\frac{M_N - M_{sun}}{M_{sun}} = -2.296 \cdot 10^{-3}$$

$$\frac{L_N - L_{sun}}{L_{sun}} = 0.131$$

$$\frac{T_{eff} - 5770}{5770} = 0.059$$

accuracy. The error is known to go as  $h^4$ , so despite its simplicity, it is surprisingly good” (Mansfield, V. 1999). that the Runge-Kutta method provided the numbers we expect. First, we show a simple relative error check to see that the mass, luminosity and temperature given numerically match up with accepted values. The Simpson method shown below

$$\frac{m_{simp} - M_N}{M_N} = -1.079 \cdot 10^{-11}$$

$$\frac{l_{simp} - L_N}{L_N} = 3.812 \cdot 10^{-11}$$

$$\frac{t_{simp} - T_N}{T_N} = -3.432 \cdot 10^{-8}$$

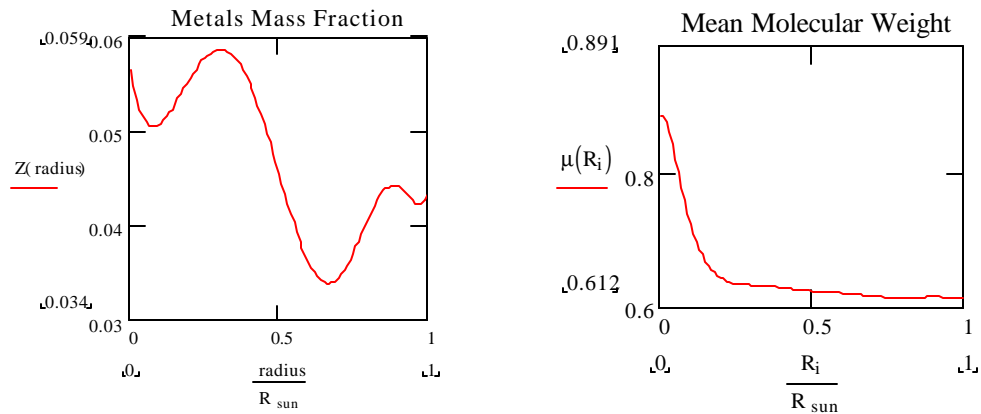
## II. Solar Chemistry

Implementation of a varying chemical composition led to a dramatically improved representation of surface characteristics. The constant chemical composition solar model solution indicates that the final luminosity is  $4.342E33$  erg/s, resulting in a  $T_{effective}$  of 5955 K. The final mass solution was shown to be

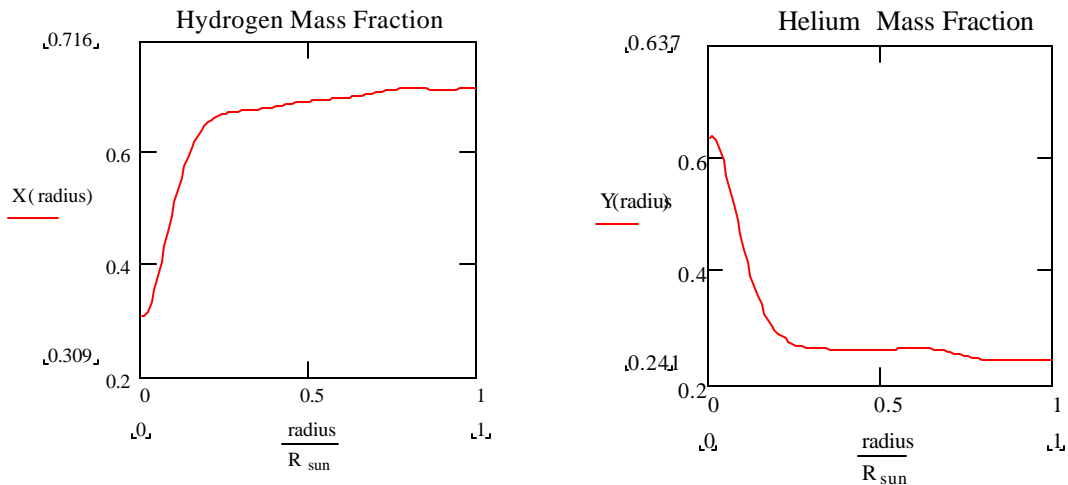
2.077E33 g. These values are all in conflict with the literature values ( $L=3.846E33$  erg/s;  $T_{\text{eff}}=5778$  K,  $M=1.989E30$  g). The star with variable chemical composition gave a final luminosity of  $3.824E33$  erg/s, resulting in a  $T_{\text{effective}}$  of 5769 K. The final mass was shown to be  $1.989E33$  g. These solutions are in excellent agreement with the literature values.

The mass fractions of hydrogen and helium were extracted from a graph of the mass fractions of the sun. It was assumed that the textbook correctly defined the mass fractions of hydrogen and helium. The functions were introduced by picking points from the mass fraction vs. radius plot given by the book. The points were graphed (for hydrogen and helium) and fit using Microcal Origin to generate two 9<sup>th</sup> order polynomials. The equation for the mass fraction of metals was defined to be the mass fraction of hydrogen and the mass fraction of helium both subtracted from unity. These mass fraction functions were introduced as functions of radius and were not solved since the solution was known beforehand. The intercepts for the polynomials were adjusted (effectively changing the initial mass fraction conditions to suit the surface conditions) from the values given in the textbook. The starting values for the model were 0.31 for hydrogen and 0.6335 for helium, and this left a starting value of 0.0565 for the metals. The textbook indicates that starting values for mass fractions are 0.336 for hydrogen and 0.643 for helium. In this case, this model is in close agreement with more sophisticated models.

The constant composition model utilizes a hydrogen mass fraction of approximately 0.7 and a helium mass fraction of approximately 0.3. Clearly this assumption is inaccurate for the core since the dominant energy source in the sun is the proton-proton chain, resulting in a depleted hydrogen concentration. A constant chemical composition assumption may be good for a young star, but even then the hydrogen would have been mildly depleted in the core.



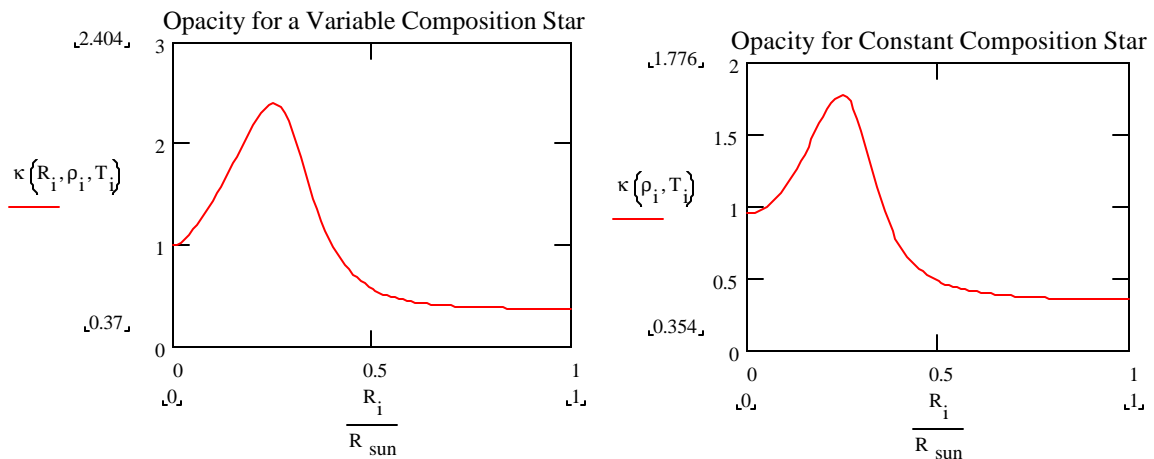
Shown above and below are curves describing the varying chemical composition.



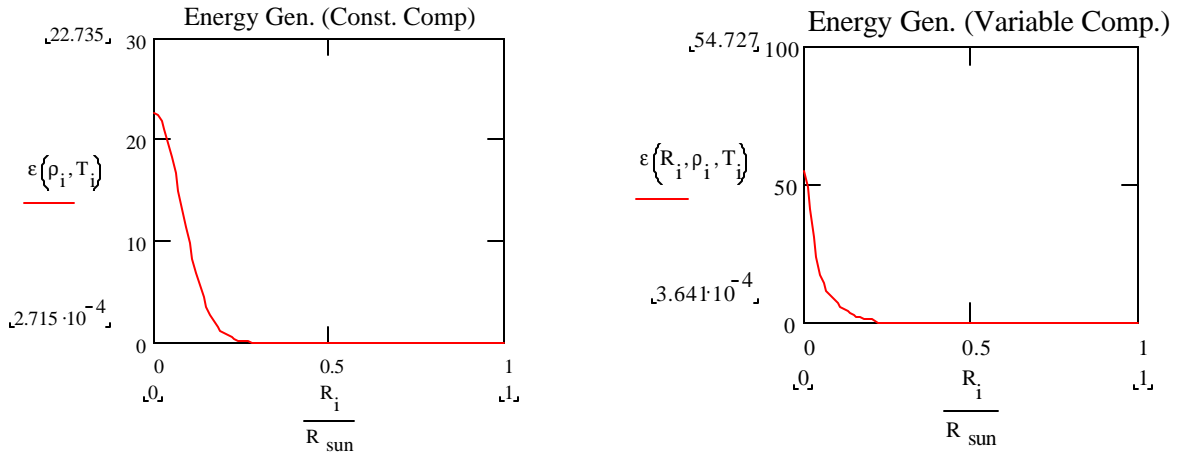
$$\epsilon_{pp}(\rho, T) := 2.38 \cdot 10^6 \cdot \rho \cdot X^2 \cdot \left\{ \frac{T}{1 \cdot 10^6} \right\}^{\frac{-2}{3}} \cdot e^{-33.8 \cdot \left\{ \frac{T}{1 \cdot 10^6} \right\}^{\frac{-1}{3}}}$$

The effect of introduced variable composition was pronounced. One severe limitation of constant composition was the starting density value. Without variable composition, starting densities greater than approximately  $111 \text{ g/cm}^3$  resulted in a failure to converge to a solution. Introduction of depleted core hydrogen concentrations allowed for the starting density to leap to approximately  $165 \text{ g/cm}^3$ , which much more accurately emulated realistic models. This is likely a result of the effect of density and temperature on the rate of nuclear energy generation, given by equation 6 for the proton-proton chain (the CNO cycle equation has the same density dependence and is not shown here). The dependence of the energy generation rate goes as the square of the hydrogen mass fraction, but only linearly with the density. A strong depletion of the central hydrogen can then support higher starting densities of hydrogen.

The opacity function in the variable composition star peaks at a value of approximately 2.5 at 0.25 solar radii. The constant composition solar model has a peak opacity value of approximately 1.8 at a radius of 0.25 solar radii. The variable composition star utilizes a smaller guillotine factor (66 instead of 100). The guillotine factor describes the contribution of an atom to the opacity after ionization (Carroll and Ostlie, p 274). The lower value of 66 was used to make the solar model consistent with observed surface characteristics by increasing an atom's opacity after ionization. The fact that the opacity is greater in the variable composition star is due to the addition of the opacity of the ionized atoms. The metal mass fraction in the variable composition star reaches a maximum at approximately the same radius as the maximum opacity, and this may contribute to the opacity maximum. The opacity graphs are presented below.



The variable composition plays an important role in the energy generation rate. The constant composition model suggests a distended core, with a gradually sloping energy generation rate. In the variable composition star, the energy generation rate begins much higher than in the constant composition model and drops off more quickly. The graphs are given below.



This could be due to the higher starting temperature ( $1.475\text{E}7$  vs.  $1.71\text{E}7$  K) of the variable composition model. The energy generation rate is extremely temperature sensitive, and a higher starting temperature can make a very large difference in the energy generation rate. It is unlikely that composition can directly cause the energy generation rate excess in the variable composition star, but the indirect temperature and density influence can explain the higher rate and steeper curve.

### III. Massive, Convecting Star

Although convection led to negligible changes in the solar model, it proved to be crucial to the transport of energy in supermassive, hot stars. It is interesting to note here that the Vogt-Russell Theorem reads that the mass and composition of a star uniquely determine its radius, luminosity, and internal structure, as well as its subsequent evolution. With this in mind, a model of a much larger star was constructed for comparative purposes. For our model of the Sun, we assumed that the changing temperature according to the radius was not dependent upon the process of convection. This proved to be a safe assumption for the sun, however for a more massive star, this is not a valid assumption. It was necessary to alter the model, as it was discovered that a more massive star relies on convection rather than radiative transfer to transport energy. It was also necessary to reconsider the composition of the star. A larger star would have a mass fraction of hydrogen that was significantly less than our Sun, so the Hydrogen mass fraction was set to sixty-five percent.

A new matrix was developed to account for the possibility of convection occurring, with a program to determine when and if the matrix should rely on the radiative transfer or convection.

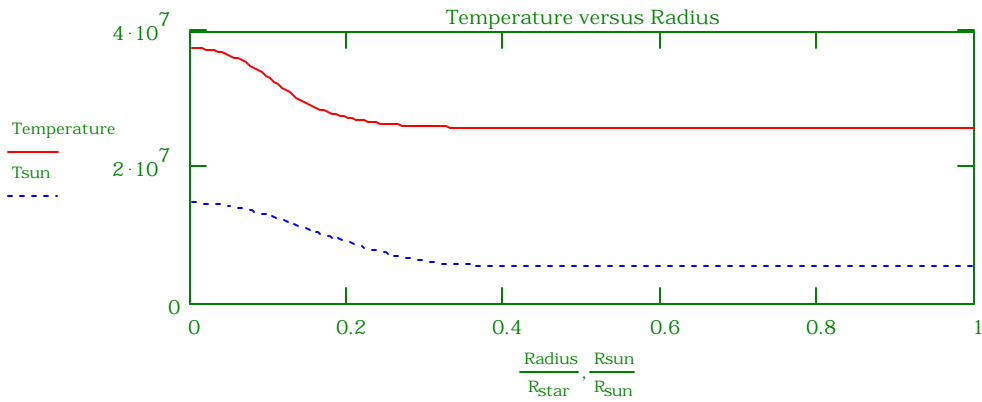
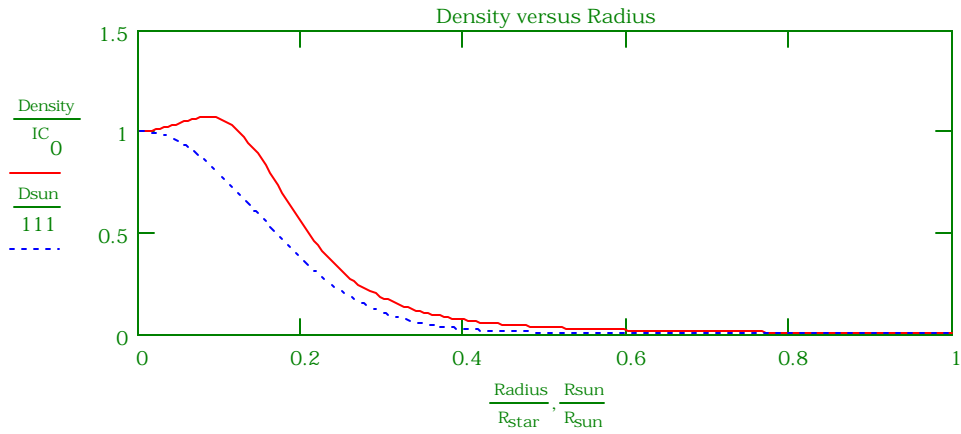
The only newly defined variables were the interior density (2.15), the interior temperature ( $3.75 \cdot 10^7$ ), and the radius of 10 R(sun). This more massive star was found to be almost completely convective. In other words, radiative transport plays a small role in energy

$$\text{Conv}_{\text{ratio}}(r, \rho, M, L, T) := \frac{\text{Temp}_{\text{rad}}(r, \rho, L, T)}{\text{Temp}_{\text{conv}}(r, M)}$$

$$dTdr(r, \rho, M, L, T) := \begin{cases} \text{Temp}_{\text{rad}}(r, \rho, L, T) & \text{if } \text{Conv}_{\text{ratio}}(r, \rho, M, L, T) < 1 \\ \text{Temp}_{\text{conv}}(r, M) & \text{if } \text{Conv}_{\text{ratio}}(r, \rho, M, L, T) \geq 1 \end{cases}$$

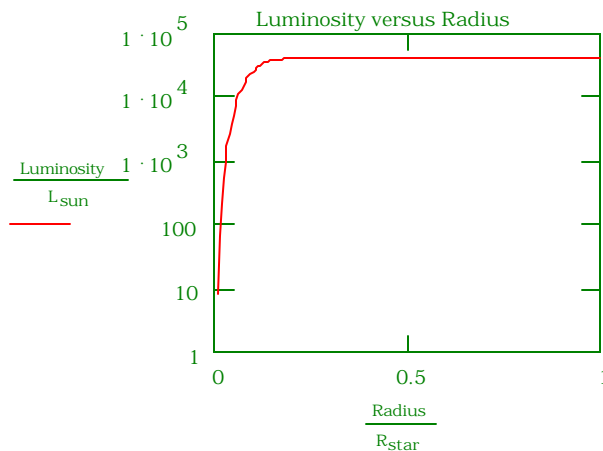
$$D(r, s) := \frac{\frac{\mu \cdot m_H}{k_b \cdot s_3} \left[ \frac{-G \cdot s_1 \cdot s_0}{r^2} + \left[ \frac{k_b \cdot s_0}{\mu \cdot m_H} + \frac{4}{3} \cdot a \cdot (s_3)^3 \right] \cdot \frac{3 \cdot \kappa(s_0, s_3) \cdot s_0 \cdot s_2}{4 \cdot a \cdot c \cdot (s_3)^3 \cdot 4 \cdot \pi \cdot r^2} \right]}{4 \cdot \pi \cdot r^2 \cdot s_0 + 4 \cdot \pi \cdot r^2 \cdot s_0 \cdot \epsilon(s_0, s_3) + dTdr(r, s_0, s_1, s_2, s_3)}$$

transport compared to adiabatic convection. Below are the results compared to the Sun...

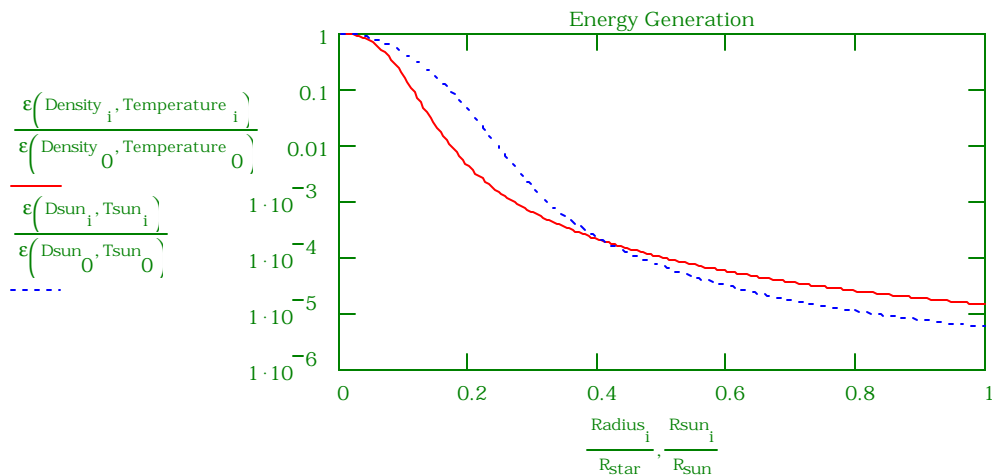


The density as compared to the density of the Sun shows the difference between our Sun and a hotter, more massive star. While the Sun did not produce such an obvious ‘hump’, the more massive star shows this aspect of stellar structure. Near the core, where the temperature and the pressure are sufficient,  $dp/dr$  is positive, so the density just outside the core increases. When the temperature begins to fall and the interior mass begins to rise, the  $dp/dr$  begins to fall again.

The graph of the temperature is normalized to the Sun and shows how the temperature varies with radius. It is almost entirely dependent on convective transport. However it is not too exciting as we can see the sun has a very similar drop off, only at a lower temperature.



The graph of the luminosity shows an odd flattening out after a short distance out of the core. This is due to the fact that the outer regions are not hot enough for the CNO cycle to continue taking place.



The graph of nuclear energy generation shows how the most fusion takes place in the core, as seen by the fall-off of the graph so sharply. The solid line is the larger star, with the dashed line representing the sun. Differences can be seen in the normalized energy generation graph with the massive star having much more intense energy generation in the core than the Sun.

One cannot believe these graphs without some sort of error analysis. The same method of Simpson's Integration was applied to this model as was the solar model. The internal consistency was found to be on the order of  $1 \cdot 10^{-5}$ .

## IV. Conclusions

The convective solar model shows that the sun has neither the temperature nor the metals mass fraction needed to increase the opacity enough to make convection an efficient means of energy transport. The exclusion of convection from the solar model was then a justified simplification to meet surface observables. Accuracy without the implementation of a varying chemical composition was modest, but the inclusion of even a basic composition model allowed for significant increases in accuracy. Mass, luminosity, and temperature all converged to observed values to within fractions of a percent, and this was accomplished with more reasonable starting conditions.

In the massive stellar model, it has been shown that the convective pathway of energy transport is crucial. This is in part a result of the hugely increased radiation pressure outside of the core, which pushes material forcibly in a way that lower temperature stars cannot. The authors' expectations were met in this since: convection was not presumed to be an important mechanism for energy transport in solar-type stars.

Although the opacity functions used in these models is primitive in comparison to research-grade models, it was still adequate to demonstrate the importance of convection and the impacts a convective core have on the outer layers (the mass, density, luminosity, and opacity functions). In addition, although the chemical composition functions were extracted from a book that generated them through another model, the effects of varying composition are immediately noticeable in the energy generation rate of the core.

Improvements could be made in the use of a more sophisticated opacity function and a more flexible chemical composition function. Regardless, in all three cases, these approximations have shown themselves to be highly instructive.

## V. Acknowledgements

We would like to thank Professor Victor Mansfield (Colgate University) for his guidance and teaching. The easy implementation of Mathsoft's Mathcad 8.0 software in the classroom is also notable.

## VI. References

Carroll, BW and DA Ostlie. *An Introduction to Modern Astrophysics*. Addison-Wesley Publishing, Reading, MA, 1996.

Mansfield, V. Personal communication. 1999.